Chemical Engineering Journal 97 (2004) 183–194

Chemical Engineering Journal

www.elsevier.com/locate/cej

Dynamic behavior of two-phase systems in physical equilibrium

M.E.E. Abashar*

Department of Chemical Engineering, College of Engineering, King Saud University, PO Box 800, Riyadh 11421, Saudi Arabia

Received 24 January 2003; accepted 9 June 2003

Abstract

The steady state and dynamic behavior of two-phase systems in physical equilibrium is investigated. The autonomous and non-autonomous systems are considered. The pseudo-arclength bifurcation technique reveals steady state multiplicity patterns not previously observed, including isola and mushroom patterns. It is shown that degenerate singular points of codimension 2, which violate the non-singularity and transversality conditions of the classical Hopf theorem exist.

The effect of the forcing amplitude and frequency on the behavior of the non-autonomous system is investigated at a number of chosen positions of the center of forcing. It is found that the forced system is very sensitive to the position of the center of forcing relative to Hopf bifurcation points of the unforced system. The excitation diagram shows that a period doubling region may exist at the top of a 2/1 resonance horn. It is shown that a Hopf bifurcation curve of the stroboscopic map is originated at bifurcation points having double −1 Floquet multipliers.

Keywords: Bifurcation; CSTR; Forced systems; Multi-phase systems; Steady state

1. Introduction

Most reactions of importance in chemical industry are mainly heterogeneous systems [1]. Large classes of these reactions such as nitrations, sulfonations and alkylations are carried out in two fluid phases [2]. Continuous stirred tank reactors are widely used in these operations. The rational design and control of such reactors require fundamental understanding of their dynamic behavior.

The literature on the dynamic behavior of the continuous stirred tank reactors of homogeneous systems is very extensive [3–8]. However, for multi-phase systems the literature is limited [9]. This is could be due to the fact that in multi-phase systems the hydrodynamic is very complex as well as the interaction of mass and heat transport and chemical reactions [10–14]. In comprehensive articles, Schmitz and Amundson [2,15] created models, which simulate the physical rate processes of heat and mass transfer between phases of perfectly mixed two-phase systems. The authors, inspired by the graphical work of Van Heerden [16] used the models to analyze the multiplicity and stability of steady state solutions of perfectly mixed two-phase systems in physical equilibrium. Only three steady states at certain parameters were presented. Linearization approach was implemented elegantly to analyze the stability criteria.

Chemical reactors exhibit a wealth of non-linear phenomena such as steady state multiplicity, quasi-periodicity and chaos. Chemical engineers have become much interested to study the features of the steady state multiplicity of reacting systems in multi-parameter space using bifurcation analysis [17–25]. The objective of bifurcation theory is to describe any sudden qualitative changes in the behavior of a system as a control parameter is smoothly varied. For example, a reactor at steady state might give way to a periodic oscillation or chaotic behavior as the feed temperature increases. The possibilities of changes are obtained in form of bifurcation diagrams. To know the state of a system at any time implies knowledge of the paths taken or not taken. It is also known that the non-linear phenomena can be very useful or harmful to the chemical processes. For example, chaos is developed through sequences of bifurcations. This non-linear phenomenon can be utilized in combustion applications to enhance the mixing of air and fuel and thus leading to an improved performance. Chaotic regions can be used to offer great flexibility to operate chemical systems due to an infinite number of unstable attractors embedded in a chaotic attractor which can be stabilized according to one's wishes. On the other hand, chaotic regions can be very harmful to stability and control of chemical processes. For example the butterfly effect, which can be produced by small unintentional disturbances can render our long term predictions of the performance of chemical processes. Moreover, unsteady state operations have been the object of much attention,

* Fax: +966-1-4678-770.
E-mail address: mabashar@ksu.edu.sa (M.E.E. Abashar).

1385-8947/$ – see front matter © 2003 Elsevier B.V. All rights reserved.
doi:10.1016/S1385-8947(03)00180-3

Nomenclature

a	forcing amplitude
C_A	overall molar concentration of component A (kmol/m^3)
C_P	overall heat capacity (kJ/kmol K)
C_P^i	heat capacity of phase i (kJ/kmol K)
D_a^i	Damköhler number of phase i
E^i	Activation energy in phase i (kJ/kmol)
F	total molar flow rate (kmol/s)
F_A	total molar flow rate of component A (kmol/s)
F^i	molar flow rate of phase i (kmol/s)
$-\Delta H_R$	heat of reaction (kJ/kmol)
k^i	reaction rate constant in phase i (s^{-1})
k_o^i	pre-exponential factor in phase i (s^{-1})
K_A	distribution coefficient of component A
N	total number of moles inside the reactor (kmol)
N^i	number of moles of phase i (kmol)
N_A	number of moles of component A inside the reactor (kmol)
P	dimensionless forcing period
P_o	dimensionless natural period of the autonomous limit cycle
q	volumetric flow rate (m^3/s)
r	ratio of an overall quantity in exit stream to that of reactor contents
R	ideal gas constant (kJ/kmol K)
t	time (s)
T	temperature inside the reactor (K)
T_c	cooling coil temperature (K)
T^i	temperature of phase i (K)
T^*	temperature rise if all of entering A were reacted adiabatically (K)
U	product of overall heat transfer coefficient to area of cooling coil (kmol/s K)
U'	dimensionless heat transfer coefficient
v	overall molar volume (m^3/kmol)
v^i	molar volume of phase i (m^3/kmol)
V	reactor volume (m^3)
V^i	volume of phase i (m^3)
$\mathbf{x}$	vector of state variables
x_A^i	mole fraction of component A in phase i
X	dimensionless overall concentration of component A
y^i	mole fraction of solvent i
y_A	overall mole fraction of component A
Y	dimensionless temperature
Y_c	dimensionless cooling coil temperature
Y_o	dimensionless overall temperature of the feed
Y_o^i	dimensionless feed temperature of phase i
Z^i	volume fraction of phase i

Greek letters

γ^i	dimensionless activation energy in phase i
ε	ratio of the holding times
θ	dimensionless time
$\boldsymbol{\lambda}$	vector of system parameters
τ	total holding time (s)
τ^i	holding time of phase i (s)
ϕ	molar ratio of the phases in the reactor
ψ	ratio of volumetric heat capacity of reactor contents to volumetric heat capacity of the feed
ω	forcing frequency (rad/s)
ω_o	natural frequency of the autonomous limit cycle (rad/s)

Subscripts

c	coolant
e	exit conditions
o	feed conditions

Superscripts

cf	center of forcing
α	phase α
β	phase β

especially with respect to the enhancement of the yield of the desire products and the reactor stability and control [25–30].

The recent concepts and modes of thought of non-linear dynamics have been implemented in this study to increase our understanding of two-phase systems in physical equilibrium and to reveal the non-linear phenomena that might exist. In this paper, we are treating the same problem of the two-phase systems in physical equilibrium presented by Schmitz and Amundson [2]. We seek to investigate more dynamic features of the two-phase systems by implementing the bifurcation analysis. First, we analyze the multiplicity and stability characteristics of the autonomous (unforced) system making use of the numerical bifurcation package AUTO [31], which based on the pseudo-arclength continuation technique. Second, we have one step further in the analysis by considering the non-autonomous (forced) system in which the basic state is a periodic operation. We analyze the forced system making use of the stroboscopic map and excitation diagrams [25–30]. The techniques to be used here seem to have capabilities to open the possibility for significant new results.

2. Transient model

The problem investigated is that of a single, first order, exothermic reaction:

$$A \rightarrow R$$

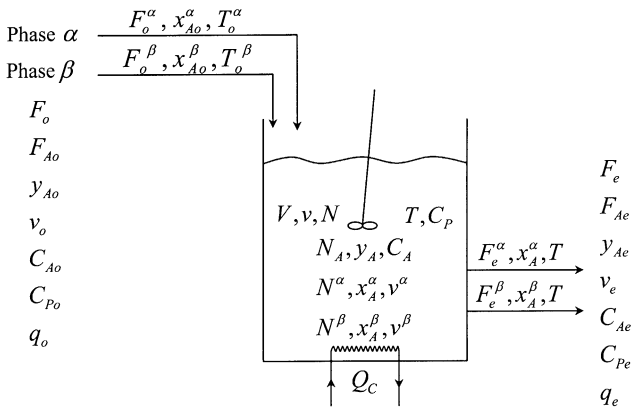

Fig. 1. Schematic representation of the continuous stirred tank reactor.

taking place in a CSTR into which liquid phases α and β are fed continuously. The specific reaction rate constants in phase α and β are given by

$$k^\alpha(T) = k_0^\alpha \, e^{-E^\alpha/RT} \tag{1}$$

$$k^\beta(T) = k_0^\beta \, e^{-E^\beta/RT} \tag{2}$$

A schematic diagram of the reactor is shown in Fig. 1. The following simplifying assumptions are used in the derivation of the conservation equations of the model [2]:

1. The system is a dilute liquid–liquid system and the phases are completely immiscible liquids.
2. The system is perfectly mixed i.e. no distributions of any kind within the system.
3. Interfacial transfer rates are rapid and the system is in physical equilibrium.
4. The temperature of the phases is equal.
5. The reaction rate alone is controlling the rate of conversion.
6. The properties of solvents α and β are constant with respect to the temperature and concentration.
7. Heats of solution are neglected, and heat capacities are constant.

During the transient state the phases are in physical equilibrium and the components are distributed between the phases according to the following equilibrium relationship:

$$x_A^\beta = K_A x_A^\alpha \tag{3}$$

where x_A^α and x_A^β are mole fractions of component A in phases α and β, respectively.

A mass balance for component A gives

$$\frac{dN_A}{dt} = (F_o^\alpha x_{Ao}^\alpha + F_o^\beta x_{Ao}^\beta) - (F_e^\alpha x_A^\alpha + F_e^\beta x_A^\beta) - (k^\alpha N^\alpha x_A^\alpha + k^\beta N^\beta x_A^\beta) \tag{4}$$

and a heat balance for the reactor gives

$$\frac{dNC_PT}{dt} = (F_o^\alpha C_P^\alpha T_o^\alpha + F_o^\beta C_P^\beta T_o^\beta) + (-\Delta H_R)(k^\alpha N^\alpha x_A^\alpha + k^\beta N^\beta x_A^\beta) - (F_e^\alpha C_P^\alpha + F_e^\beta C_P^\beta)T - U(T - T_c) \tag{5}$$

where subscripts o and e refer to the feed and exit streams, respectively; N_A and N the total moles of component A and the two phases in the reactor, respectively; F the molar flow rate; N^α and N^β the moles of the α and β phases in the reactor, respectively; U the product of an overall heat transfer coefficient and a surface area.

The changes in the amount of the solvents α and β are given by the following transient equations:

$$\frac{dN^\alpha}{dt} = F_o^\alpha - F_e^\alpha \tag{6}$$

$$\frac{dN^\beta}{dt} = F_o^\beta - F_e^\beta \tag{7}$$

The total volume of the system is constant, then

$$\frac{dV}{dt} = v^\alpha \frac{dN^\alpha}{dt} + v^\beta \frac{dN^\beta}{dt} = 0 \tag{8}$$

where v^α and v^β are the molar volumes of the α and β phases, respectively.

The holding time for each phase is defined by

$$\tau^\alpha = \frac{N^\alpha}{F_o^\alpha}, \qquad \tau^\beta = \frac{N^\beta}{F_o^\beta} \tag{9}$$

and the ratio of the holding times is given by

$$\varepsilon = \frac{\tau^\alpha}{\tau^\beta} \tag{10}$$

and the molar ratio of the phases in the reactor is defined as

$$\phi = \frac{N^\beta}{N^\alpha} \tag{11}$$

Experiments have shown that the ratio of the phases in the reactor is an independent parameter [2,32] and may be related to exit the flow rates as

$$\frac{F_e^\beta}{F_e^\alpha} = \varepsilon \frac{N^\beta}{N^\alpha} = \varepsilon\phi \tag{12}$$

In two-phase systems, overall quantities inside the reactor are not equal to overall quantities leaving the reactor. Based on the above relations, the overall mole fraction of component A (y_A), overall molar volume (v), overall concentration of A (C_A) and the overall heat capacity (C_P) within the reactor are given by

$$y_A = \frac{N_A}{N} = \frac{N^\alpha x_A^\alpha + N^\beta x_A^\beta}{N^\alpha + N^\beta} = \frac{x_A^\alpha + \phi x_A^\beta}{1+\phi} = \frac{x_A^\alpha(1+\phi K_A)}{1+\phi} \tag{13}$$

$$v = \frac{V}{N} = \frac{N^{\alpha}v^{\alpha} + N^{\beta}v^{\beta}}{N^{\alpha} + N^{\beta}} = \frac{v^{\alpha} + \phi v^{\beta}}{1+\phi} \tag{14}$$

$$C_{\mathrm{A}} = \frac{N_{\mathrm{A}}}{V} = \frac{N^{\alpha}x_{\mathrm{A}}^{\alpha} + N^{\beta}x_{\mathrm{A}}^{\beta}}{V} = \frac{x_{\mathrm{A}}^{\alpha}(1+\phi K_{\mathrm{A}})}{v^{\alpha} + \phi v^{\beta}} = \frac{y_{\mathrm{A}}}{v} \tag{15}$$

$$C_P = \frac{N^{\alpha}C_P^{\alpha} + N^{\beta}C_P^{\beta}}{N^{\alpha} + N^{\beta}} = \frac{C_P^{\alpha} + \phi C_P^{\beta}}{1+\phi} \tag{16}$$

Similarly at the exit of the reactor

$$y_{\mathrm{Ae}} = \frac{F_{\mathrm{Ae}}}{F_{\mathrm{e}}} = \frac{F_{\mathrm{e}}^{\alpha}x_{\mathrm{A}}^{\alpha} + F_{\mathrm{e}}^{\beta}x_{\mathrm{A}}^{\beta}}{F_{\mathrm{e}}^{\alpha} + F_{\mathrm{e}}^{\beta}} = \frac{x_{\mathrm{A}}^{\alpha} + \varepsilon\phi x_{\mathrm{A}}^{\beta}}{1+\varepsilon\phi} = \frac{x_{\mathrm{A}}^{\alpha}(1+\varepsilon\phi K_{\mathrm{A}})}{1+\varepsilon\phi} \tag{17}$$

$$v_{\mathrm{e}} = \frac{q_{\mathrm{e}}}{F_{\mathrm{e}}} = \frac{F_{\mathrm{e}}^{\alpha}v^{\alpha} + F_{\mathrm{e}}^{\beta}v^{\beta}}{F_{\mathrm{e}}^{\alpha} + F_{\mathrm{e}}^{\beta}} = \frac{v^{\alpha} + \varepsilon\phi v^{\beta}}{1+\varepsilon\phi} \tag{18}$$

$$C_{\mathrm{Ae}} = \frac{F_{\mathrm{Ae}}}{q_{\mathrm{e}}} = \frac{F_{\mathrm{e}}^{\alpha}x_{\mathrm{A}}^{\alpha} + F_{\mathrm{e}}^{\beta}x_{\mathrm{A}}^{\beta}}{F_{\mathrm{e}}^{\alpha}v^{\alpha} + F_{\mathrm{e}}^{\beta}v^{\beta}} = \frac{x_{\mathrm{A}}^{\alpha}(1+\varepsilon\phi K_{\mathrm{A}})}{v^{\alpha} + \varepsilon\phi v^{\beta}} = \frac{y_{\mathrm{Ae}}}{v_{\mathrm{e}}} \tag{19}$$

$$C_{P\mathrm{e}} = \frac{F_{\mathrm{e}}^{\alpha}C_P^{\alpha} + F_{\mathrm{e}}^{\beta}C_P^{\beta}}{F_{\mathrm{e}}^{\alpha} + F_{\mathrm{e}}^{\beta}} = \frac{C_P^{\alpha} + \varepsilon\phi C_P^{\beta}}{1+\varepsilon\phi} \tag{20}$$

Let the symbol r will be used to designate the ratio of an overall quantity in the exit stream to that inside the reactor, then

$$r_y = \frac{y_{\mathrm{Ae}}}{y_{\mathrm{A}}} == \frac{(1+\varepsilon\phi K_{\mathrm{A}})(1+\phi)}{(1+\phi K_{\mathrm{A}})(1+\varepsilon\phi)} \tag{21}$$

$$r_v = \frac{v_{\mathrm{e}}}{v} = \frac{(1+\varepsilon\phi v^{\beta}/v^{\alpha})(1+\phi)}{(1+\phi v^{\beta}/v^{\alpha})(1+\varepsilon\phi)} \tag{22}$$

$$r_{C_P} = \frac{C_{P\mathrm{e}}}{C_P} = \frac{(1+\varepsilon\phi C_P^{\beta}/C_P^{\alpha})(1+\phi)}{(1+\phi C_P^{\beta}/C_P^{\alpha})(1+\varepsilon\phi)} \tag{23}$$

Let y^{α} and y_{e}^{α} and will be used as the mole fraction of solvent α inside the reactor and in the exit stream, respectively. Then

$$y^{\alpha} = \frac{N^{\alpha}}{N} = \frac{N^{\alpha}}{N^{\alpha} + N^{\beta}} = \frac{1}{1+\phi} \tag{24}$$

$$y_{\mathrm{e}}^{\alpha} = \frac{F_{\mathrm{e}}^{\alpha}}{F_{\mathrm{e}}} = \frac{F_{\mathrm{e}}^{\alpha}}{F_{\mathrm{e}}^{\alpha} + F_{\mathrm{e}}^{\beta}} = \frac{1}{1+\varepsilon\phi} \tag{25}$$

$$r_{\alpha} = \frac{y_{\mathrm{e}}^{\alpha}}{y^{\alpha}} = \frac{1+\phi}{1+\varepsilon\phi} \tag{26}$$

if the densities of the phases are constant, the volumetric flow rates at the inlet (q_{o}) and exit (q_{e}) of the reactor should be the same. Thus

$$F_{\mathrm{o}}v_{\mathrm{o}} = F_{\mathrm{e}}v_{\mathrm{e}} = F_{\mathrm{e}}vr_v \tag{27}$$

and the total holding time is given by

$$\tau = \frac{V}{q_{\mathrm{o}}} = \frac{V}{F_{\mathrm{o}}v_{\mathrm{o}}} = \frac{N}{F_{\mathrm{e}}r_v} = \left(\frac{r_{\alpha}}{r_v}\right)\tau^{\alpha} = \left(\frac{r_{\beta}}{r_v}\right)\tau^{\beta} \tag{28}$$

let the ratio of volumetric heat capacity of reactor contents to volumetric heat capacity of the feed is given by

$$\psi = \frac{C_P/v}{C_{P\mathrm{o}}/v_{\mathrm{o}}} \tag{29}$$

The molar ratio of the phases (ϕ) can be expressed in terms of volume fraction (Z^{α}) of phase α as

$$\phi = \frac{N^{\beta}}{N^{\alpha}} = \frac{V^{\beta}/v^{\beta}}{V^{\alpha}/v^{\alpha}} = \frac{1-Z^{\alpha}}{(v^{\beta}/v^{\alpha})Z^{\alpha}} \tag{30}$$

where

$$Z^{\alpha} = \frac{V^{\alpha}}{V} \tag{31}$$

Now let us define the following variables and parameters:

$$X = \frac{C_{\mathrm{A}}}{C_{\mathrm{Ao}}}, \quad Y = \frac{T}{T^*}, \quad Y_{\mathrm{c}} = \frac{T_{\mathrm{c}}}{T^*}, \quad \theta = \frac{t}{\tau},$$
$$T^* = \frac{(-\Delta H_{\mathrm{R}})y_{\mathrm{Ao}}}{C_{P\mathrm{o}}}, \quad D_{\mathrm{a}}^{\alpha} = \tau k_{\mathrm{o}}^{\alpha}, \quad D_{\mathrm{a}}^{\beta} = \tau k_{\mathrm{o}}^{\beta},$$
$$\gamma^{\alpha} = \frac{E^{\alpha}}{RT^*}, \quad \gamma^{\beta} = \frac{E^{\beta}}{RT^*},$$
$$Y_{\mathrm{o}} = \frac{Y_{\mathrm{o}}^{\alpha} + \varepsilon\phi(C_P^{\beta}/C_P^{\alpha})Y_{\mathrm{o}}^{\beta}}{1+\varepsilon\phi(C_P^{\beta}/C_P^{\alpha})}, \quad U' = \frac{U}{F_{\mathrm{o}}C_{P\mathrm{o}}} \tag{32}$$

Substitutions of the above definitions reduce Eqs. (4)–(8) to

$$\frac{\mathrm{d}X}{\mathrm{d}\theta} = 1 - \left(\frac{r_y}{r_v}\right)X - \frac{D_{\mathrm{a}}^{\alpha}\,\mathrm{e}^{-\gamma^{\alpha}/Y} + D_{\mathrm{a}}^{\beta}\phi K_{\mathrm{A}}\,\mathrm{e}^{-\gamma^{\beta}/Y}}{1+\phi K_{\mathrm{A}}}X \tag{33}$$

$$\frac{\mathrm{d}(\psi Y)}{\mathrm{d}\theta} = Y_{\mathrm{o}} + \frac{D_{\mathrm{a}}^{\alpha}\,\mathrm{e}^{-\gamma^{\alpha}/Y} + D_{\mathrm{a}}^{\beta}\phi K_{\mathrm{A}}\,\mathrm{e}^{-\gamma^{\beta}/Y}}{1+\phi K_{\mathrm{A}}}X - \left(\frac{r_{C_P}}{r_v}\right)(\psi Y) - U'(Y - Y_{\mathrm{c}}) \tag{34}$$

$$\frac{\mathrm{d}Z^{\alpha}}{\mathrm{d}\theta} = Z_{\mathrm{o}}^{\alpha} - \left(\frac{r_{\alpha}}{r_v}\right)Z^{\alpha} \tag{35}$$

3. Computational techniques

The bifurcation diagrams were obtained by using the software package AUTO-86 of Doedel and Kernévez [31]. This package is able to trace out the entire stable and unstable steady state and periodic branches and locates the limit and Hopf bifurcation points. AUTO uses pseudo-arclength continuation technique to overcome the problem of tracing branches of solutions past singularities. The eigenvalues and

Floquet multipliers were computed along the branches to determine their stability properties.

A stiff differential equation solver called DGEAR from the IMSL [33] was utilized to solve the system of the ordinary differential equations (33)–(35) to obtain the phase plane and time trace diagrams. To ensure accuracy, automatic step size and double precision were used with input relative error bound of 10^{-14}.

The period of the oscillation of the natural system (unforced) was determined with high accuracy. A shooting algorithm using Newton method was employed for this purpose [25]. Consider the system of the ordinary differential equations:

$$\frac{\mathrm{d}\mathbf{x}}{\mathrm{d}\theta} = \mathbf{f}\,(\mathbf{x}, \boldsymbol{\lambda})\,, \quad \mathbf{x} \in \mathbb{R}^n \tag{36}$$

where $\mathbf{x}$ is a vector of state variables, $\mathbf{f}$ a vector of non-linear functions and $\boldsymbol{\lambda}$ a vector of system parameters. A periodic trajectory must satisfy the boundary conditions:

$$\mathbf{x}(\theta = 0) = \mathbf{x}(\theta = P_\mathrm{o}) \tag{37}$$

where P_o is the period of the limit cycle. The solution of this two-point boundary problem is equivalent to the solution of the system of equations:

$$\mathbf{F}(\mathbf{x}, P_\mathrm{o}) - \mathbf{x} = 0 \tag{38}$$

where P_o is unknown and $\mathbf{F}(\mathbf{x}, P_\mathrm{o})$ is obtained by integrating Eq. (36). Since all points on the periodic trajectory coincide after period P_o, an anchor equation of the form:

$$N(x, P_\mathrm{o}) = 0 \tag{39}$$

is utilized to eliminate free translation in time (infinity of solutions). Eqs. (38) and (39) may be solved using Newton method, where the Jacobian is given by

$$\mathbf{J} = \begin{pmatrix} \dfrac{\partial \mathbf{F}}{\partial \mathbf{x}} - \mathbf{I} & \dfrac{\partial \mathbf{F}}{\partial P_\mathrm{o}} \\ \dfrac{\partial N}{\partial x} & \dfrac{\partial N}{\partial P_\mathrm{o}} \end{pmatrix} \tag{40}$$

where $\mathbf{I}$ is the identity matrix and the derivatives $\partial\mathbf{F}/\partial\mathbf{x}$ are computed variationally.

For the forced (non-autonomous) system:

$$\frac{\mathrm{d}\mathbf{x}}{\mathrm{d}\theta} = \mathbf{f}(\mathbf{x}, \theta, \boldsymbol{\lambda}), \quad \mathbf{x} \in \mathbb{R}^n \tag{41}$$

the vector field depends explicitly on time. Excitation diagrams and stroboscopic maps are used to study the response of the forced systems [25–30]. The excitation diagrams are bifurcation diagrams of forced amplitude (a) and frequencies ($\omega/\omega_\mathrm{o} = P/P_\mathrm{o} = n/m$), where ω and ω_o are the frequencies of the forced and unforced (natural) systems, respectively. P ($=2\pi/\omega$) and P_o ($=2\pi/\omega_\mathrm{o}$) are the periods of the forced and unforced systems, respectively, and n and m are prime integers. At low forcing amplitudes and n and m are rational numbers, the periodic trajectories form frequency locking regions having periods which are an integer multiple of the forcing period (nP) and develop on a surface of a torus (doughnut-shape). This torus is the result of forcing the limit cycle of the natural system (autonomous system). The boundaries of these regions are loci of saddle-node bifurcations and called resonance horn (entrainment, sub-harmonic, Arnold tongue) regions. The excitation diagrams may have different regions of periodicity, quasi-periodicity and chaos [25,27,30].

The forcing periods ($P = (n/m)P_\mathrm{o}$) always present in the response of the forced systems and used to strobe these systems. The projections of the stroboscopic points on planes are called stroboscopic maps. The stroboscopic maps reduce the dimension of the problem e.g. the periodic trajectories present as fixed points and tori as invariant circles. Bifurcations in the excitation diagrams e.g. saddle-node, Hopf and period doubling are analyzed by computing the eigenvalues (Floquet multipliers) of periodic responses. The condition for a periodic solution may be written as

$$\mathbf{F}^k(\mathbf{x}, \boldsymbol{\lambda}) - \mathbf{x} = 0 \tag{42}$$

where $\mathbf{F}^k(\mathbf{x}, \boldsymbol{\lambda})$ is the kth iterate of the stroboscopic map. Eq. (42) may be solved by Newton–Raphson iterations and the Jacobian matrix of the stroboscopic map is given by

$$\mathbf{J}(\mathbf{x}, \boldsymbol{\lambda}) = D\mathbf{F}^k(\mathbf{x}, \boldsymbol{\lambda}) - \mathbf{I} \tag{43}$$

Since $\mathbf{F}$ is not algebraic, the Jacobian is obtained variationally by integrating the model equation (41) with the following variational equations:

$$\frac{\mathrm{d}\mathbf{B}}{\mathrm{d}\theta} = \frac{\partial \mathbf{f}}{\partial \mathbf{x}}\,[\mathbf{x}(\mathbf{x}_\mathrm{o}, \theta, \boldsymbol{\lambda}), \theta, \boldsymbol{\lambda}] \cdot \mathbf{B}, \quad \mathbf{B}(0) = \mathbf{I} \tag{44}$$

which are integrated until a time $\theta = kP$, where

$$D\mathbf{F}^k(\mathbf{x}_\mathrm{o}, \boldsymbol{\lambda}) = \mathbf{B}(kP) \tag{45}$$

upon convergence, the eigenvalues of the matrix $\mathbf{B}$ are the Floquet multipliers, which determine the bifurcation criteria of the periodic orbit. Examples of the bifurcation of the response of the forced system are saddle-node, period doubling and Hopf bifurcation of the stroboscopic map. These types of bifurcations are usually shown in the excitation diagrams.

4. Results and discussion

Since this system contains a large number of parameters, so it is a difficult task to study the entire parameter space. Therefore, we consider in this study samples of parameter spaces to reveal some of steady state and dynamic features, which may arise, in such complex multi-phase systems. The parameters used in this study are taken from the work of Schmitz and Amundson [2] and shown in Table 1.

Table 1
Data used for the continuous stirred tank reactor [2]

K_A	0.2
C_P^β / C_P^α	1.0
Uv^α / VC_P^α (s^{-1})	6.37×10^{-3}
v^β / v^α	1.0
Y_o^α	1.8
Y_o^β	1.8
γ^α	63.5
γ^β	51.5
ε	0.8

4.1. Autonomous system

Fig. 2(a) and (b) shows one-parameter bifurcation diagrams for the dimensionless overall concentration (X) and temperature (Y) inside the reactor, respectively. Damköhler number (D_a^α) of phase α is considered as the bifurcation parameter. The bifurcation diagrams clearly show the existence of a region of multiple steady state solutions between two static limit (saddle-node) points (SLP_1, SLP_2) and another region of periodic solutions between two Hopf bifurcation points (HB_1, HB_2). The system undergoes a saddle-node bifurcation, when one of the real eigenvalues passes through the origin of the complex plane i.e. the Jacobian becomes singular and a saddle point coincides with a node point. The number of the limits points is even and is known to produce the hysteresis effect (ignition and extinction phenomena). An unstable steady state branch of a saddle type connects the two limit points as shown in Fig. 2. The eigenvalues of this branch are pure real of opposite signs. The positive and the negative signs correspond to the unstable and stable manifolds enter the saddle point and are called separatrices, which separate two basins of attraction of the steady states. The Hopf bifurcation occurs when a pair of complex conjugates of eigenvalues crosses the imaginary axis transversally. At the Hopf bifurcation point periodic solutions (oscillations) appear. In our case, the periodic solution is stable because the Floquet multipliers lie within a unit circle in the complex plane. Fig. 3(a) shows a sample of a limit cycle (periodic solution) at $\ln D_a^\alpha = 29.0$, and the corresponding time trace is shown in Fig. 3(b).

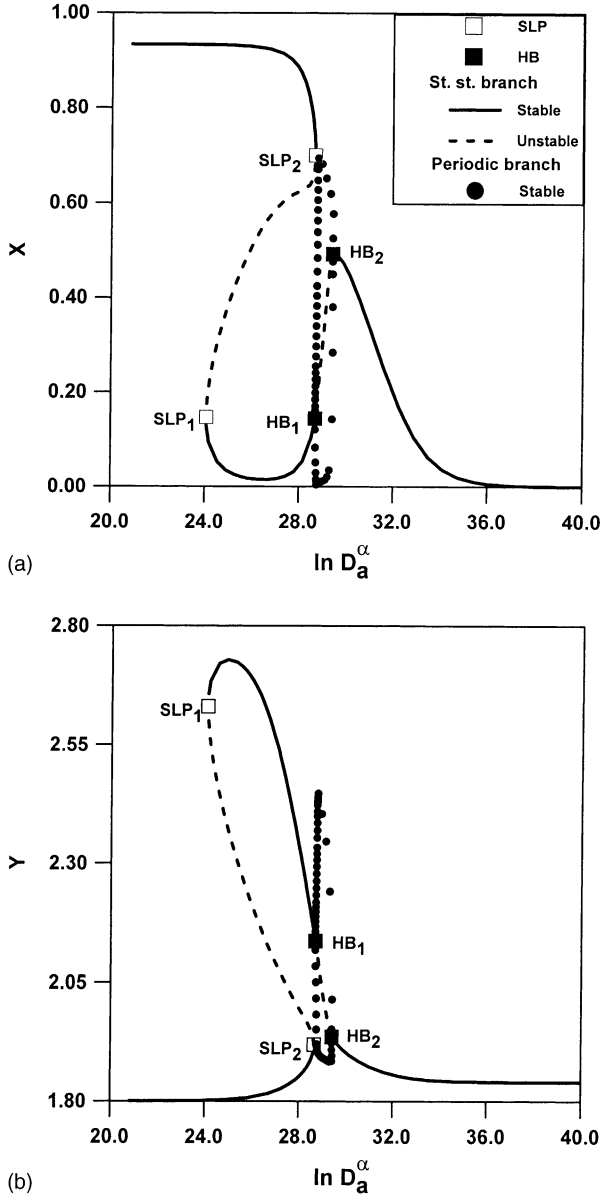

Fig. 2. One-parameter bifurcation diagram at $Y_c = 1.84$: (a) dimensionless overall concentration of component A (X) vs. $\ln D_a^\alpha$; (b) dimensionless temperature (Y) vs. $\ln D_a^\alpha$.

For further analysis the saddle-node (turning) points and the Hopf bifurcation points in Fig. 2 are used to generate a two-parameter bifurcation diagram. Fig. 4 shows the two-parameter bifurcation in (Y_c, D_a^α) space. The continuation of the static limit points is shown in Fig. 4(a). The continuation of the Hopf bifurcation points is also shown in the enlargement region presented in Fig. 4(b). The locus of the static limit points forms a cusp (singular point) of codimension 2 at $Y_c = 1.8343$. The cusp divides the plane into two steady state regions I and II, which have different steady state multiplicity patterns. The locus of the Hopf bifurcation points attains a maximum point at which two Hopf bifurcation points coincide. This maximum point is a degenerate Hopf bifurcation point, since the complex conjugate eigenvalues with real parts cross the imaginary axis tangentially i.e. violate the cross condition of the Hopf theorem [8]. The locus of the Hopf bifurcation point is also terminates on the locus of the static limit point at the cusp and at region I forming another type of degenerate bifurcation points. These types of the degenerate bifurcation points are called double zero degeneracies because the pure pair imaginary eigenvalues characterizing the Hopf bifurcation point tend to zero. The coalescence of the Hopf and the static limit points at the cusp ($Y_c =$

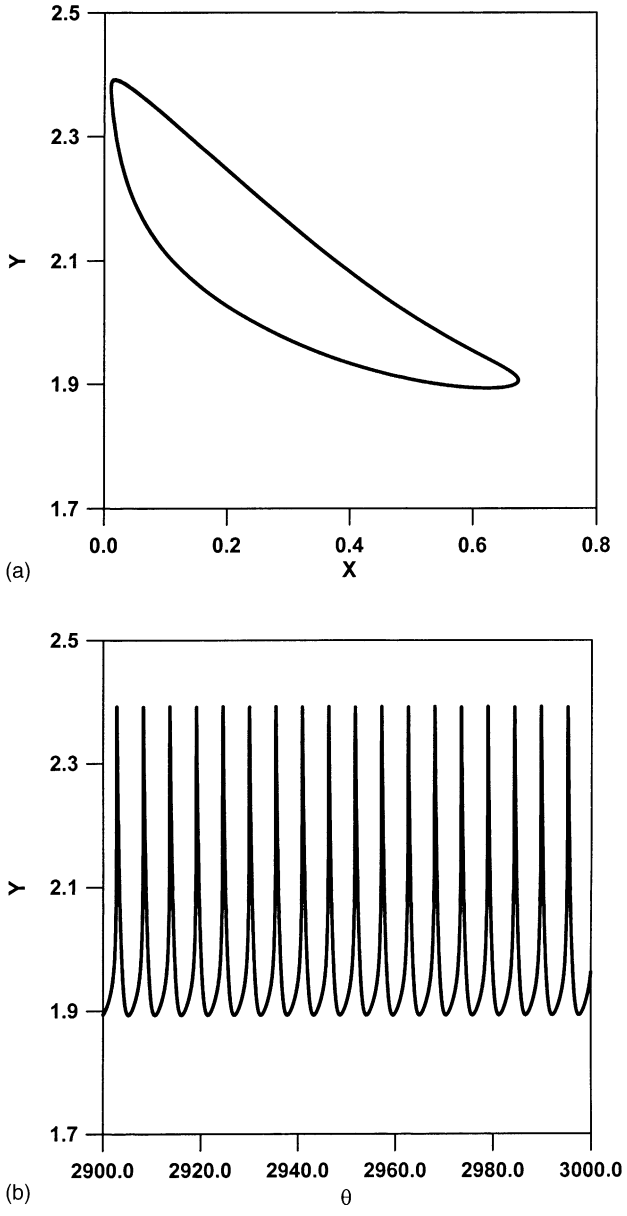

Fig. 3. Dynamic simulation of unforced reactor at $Y_c = 1.84$ and $\ln D_a^{\alpha} = 29.0$: (a) phase plane; (b) time trace.

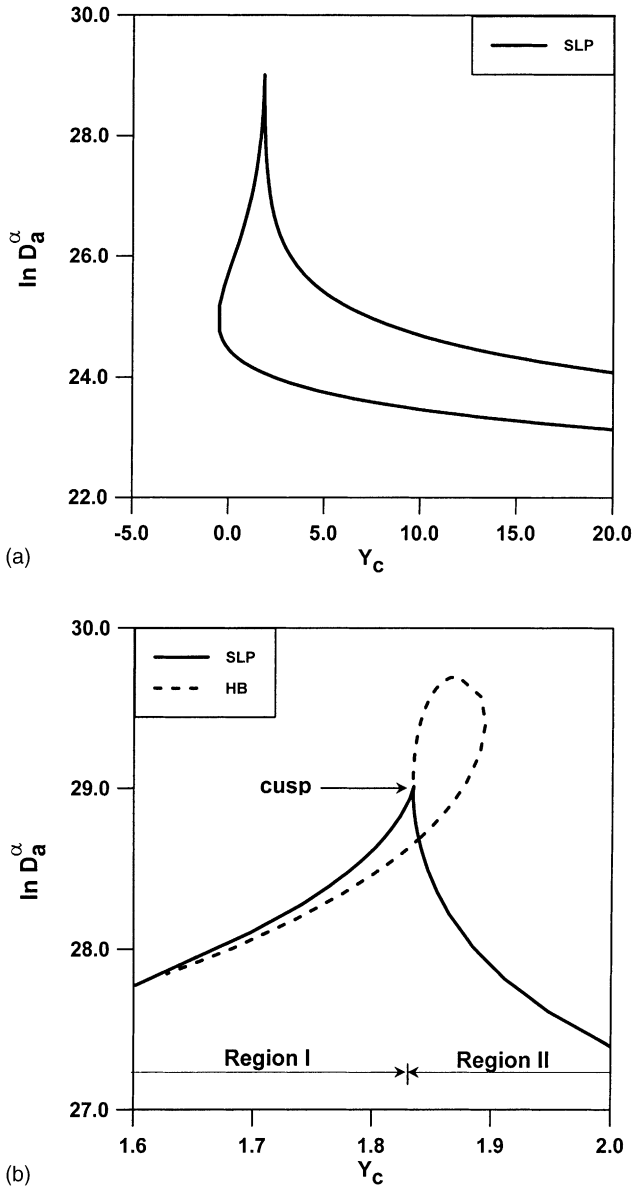

Fig. 4. Two-parameter bifurcation diagram: (a) locus of static limit points (SLP); (b) enlargement region of the loci of static limit points (SLP) and Hopf bifurcation points (HB).

1.8343) is shown in the bifurcation diagram presented in Fig. 5(a).

In general unique solutions exist in the absence of the static limits points. In region I, a unique solution and isola patterns exist. The unique solution could exist when there are no limit points (e.g. $Y_c < 0$) as shown in Fig. 4(a). The isola pattern is shown by the representative bifurcation diagram in Fig. 5(b) at $Y_c = 1.8300$. In region II, a mushroom and an S (hysteresis) pattern could exist as shown in the representative bifurcation diagrams presented in Fig. 5(c) and (d) at $Y_c = 1.8400$ and 4.0000, respectively. This implies that one can find the mushroom pattern exists in between the isola and S patterns.

4.2. Non-autonomous (forced) system

It is known that complex behavior is expected in the vicinity of degenerate singular points [25]. Fig. 6 shows a one-parameter bifurcation diagram for the autonomous (unforced) system at $\ln D_a^{\alpha} = 29.3$ in the neighborhood of the cusp point shown in Fig. 4. The forcing variable (Y_c) is chosen as a bifurcation parameter. This figure is essential because it represents the limiting case of the forced system, as the forcing amplitude tends to zero i.e. the state of the unforced (natural) autonomous system on which we impose the effect of the forcing variable.

The bifurcation diagram is divided into three regions A, B and C. Stable branches of unique steady state solutions exist

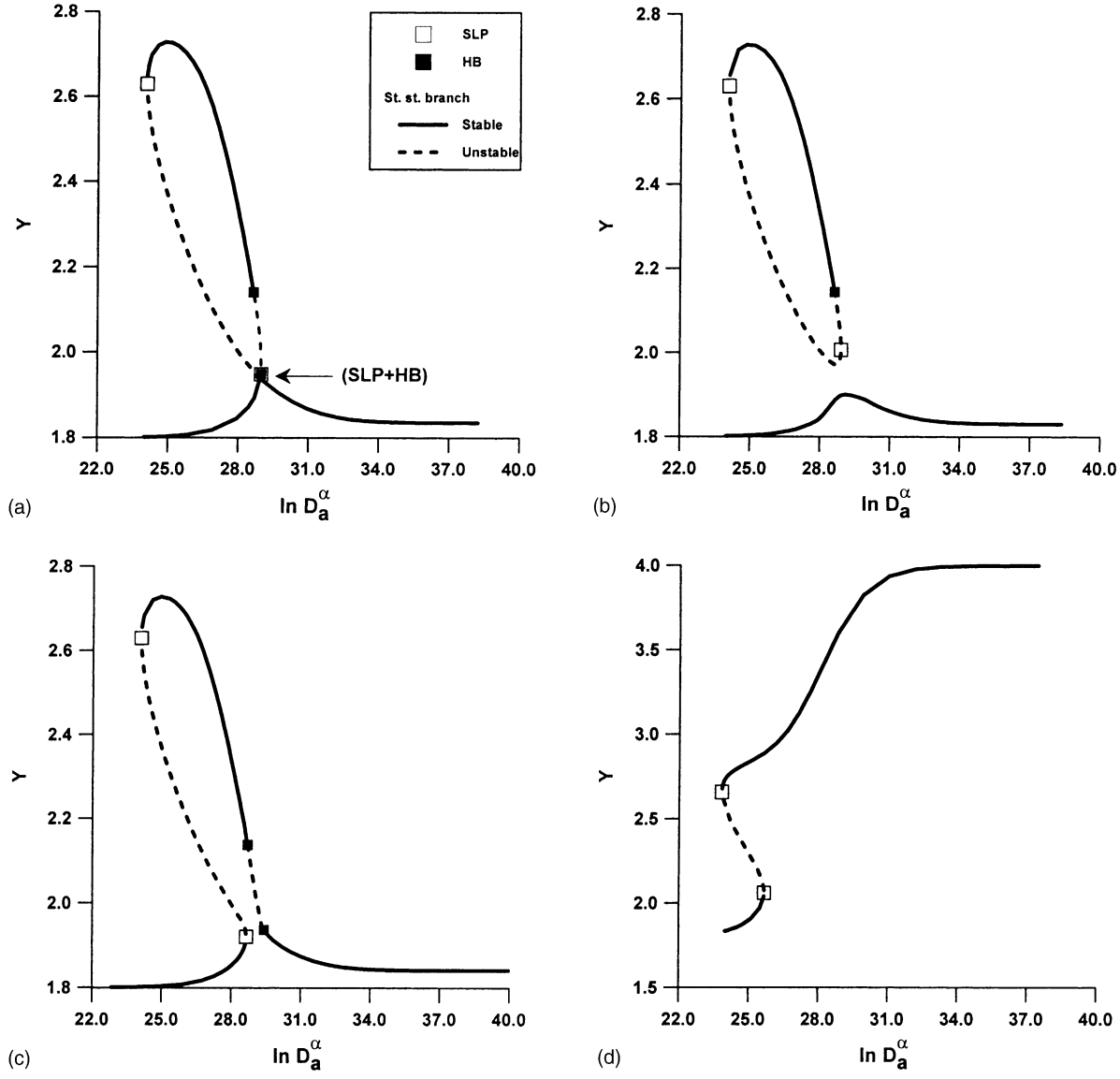

Fig. 5. One-parameter bifurcation diagram of dimensionless temperature vs. $\ln D_a^\alpha$: (a) coincidence of the cusp point and the Hopf bifurcation point at $Y_c = 1.8343$; (b) isola pattern at $Y_c = 1.8300$; (c) mushroom pattern at $Y_c = 1.8400$; (d) S-shaped patter at $Y_c = 4.0000$.

in regions A and C and a stable periodic solution originates from two Hopf bifurcation points ($HB_3 = 1.836761$, $HB_4 = 1.892585$) exists in region B.

We consider the forced reactor when the coolant temperature is changed according to

$$Y_c = Y_c^{cf} + a\sin(\omega\theta) \tag{46}$$

where Y_c^{cf} is the coolant temperature, which represents the position of the center of forcing. In this case, the system becomes a non-autonomous system since the vector field (Eqs. (33)–(35)) depends explicitly on time (θ). The limiting case (unforced reactor) chosen in this study is a full time oscillator in region B, which has a stable limit cycle surrounding an unstable steady state. The forcing cycle depends on the position of the center of forcing and the magnitude of the forcing amplitude. During the forcing cycle, we could force an oscillator alone (region B) or an oscillator plus phase planes of unique steady states when the forcing amplitude reaches the Hopf bifurcation points i.e. regions A + B, B + C or A + B + C.

The variation of the natural period (P_o) of the unforced reactor (autonomous system) with the coolant temperature (Y_c) between HB_3 and HB_4 is shown in Fig. 7. Three centers of forcing cf_1, cf_2 and cf_3 at $Y_c^{cf_1} = 1.851811$, $Y_c^{cf_2} = 1.837218$ and $Y_c^{cf_3} = 1.890070$ are considered. The case of the first center of forcing (cf_1) is considered with more details.

For the first center of forcing (cf_1) the period of oscillation of the autonomous system is $P_o = 3.085124$. Due to the infinity of the rational numbers only one representative

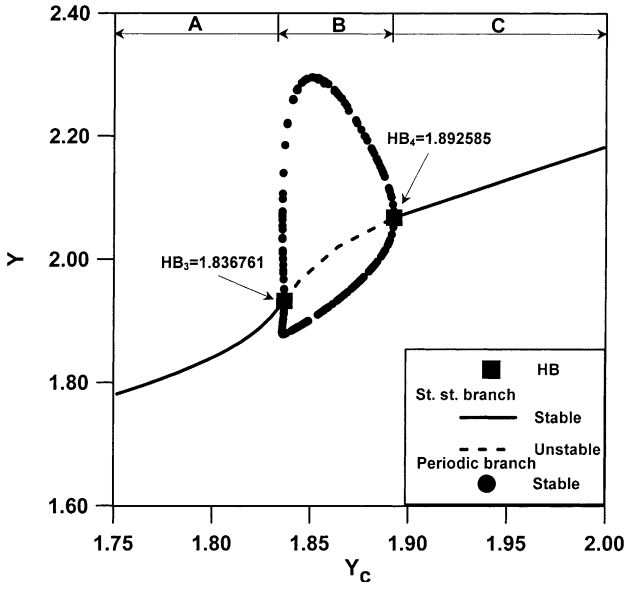

Fig. 6. One-parameter bifurcation diagram of the unforced reactor model at $\ln D_a^{\alpha} = 29.3$.

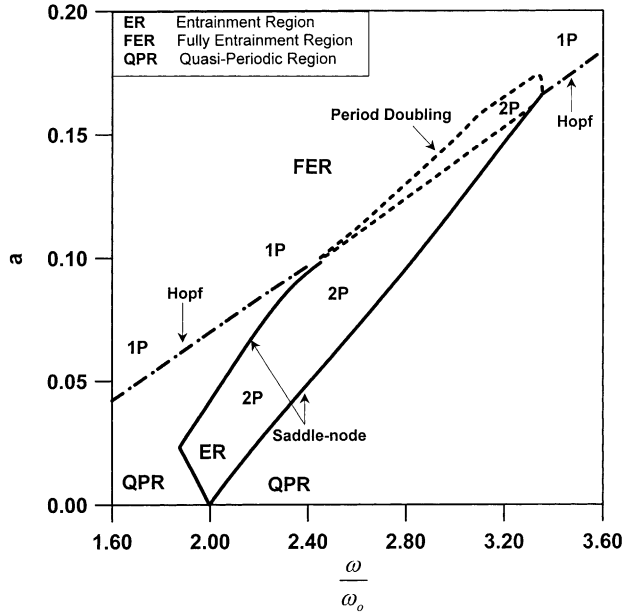

Fig. 8. Excitation diagram of the 2/1 resonance horn for the first center of forcing (cf_1) at $Y_c^{cf_1} = 1.851811$.

resonance horn with its tip at $\omega/\omega_o = P_o/P = n/m = 2/1$ is generated as shown in Fig. 8. This two-parameter excitation diagram is a function of the forcing amplitude (a) and the ratio of the forcing and natural frequencies (ω/ω_o). The diagram may be convenient to describe the expected dynamic behavior of the forced system. The possible behavior of the forced system could be periodic, quasi-periodic and chaotic [25]. Fig. 8 is divided into four regions: entrainment region (ER), quasi-periodic region (QPR), period doubling region (PDR) and fully entrainment region (FER).

The entrainment (frequency locking, sub-harmonic) region is formed at low forcing amplitude as a V-shaped resonance horn as shown in Fig. 8. At low forcing amplitude, the autonomous unstable steady state shown in Fig. 6 becomes unstable limit cycle and the limit cycle of the autonomous system becomes a two-dimensional torus [25,27,30]. This torus appears in the stroboscopic phase plane as invariant circle. Since the ratio of the frequencies is rational number ($n/m = 2/1$), a frequency locked oscillations are constrained to the surface of the torus. The period of the oscillation is locked to be an integer multiple of the forcing period i.e. $2P$ in our case. The phase-locked torus has two pairs of alternating period $2P$ saddles and nodes forming part of its boundaries. It is clearly shown that the saddle-node bifurcation curves separate the frequency locking (entrainment) region from the quasi-periodic region that exists outside the resonance horn. At the saddle-node bifurcation points, a Floquet multiplier passes out the unit circle through $+1$ i.e. an unstable periodic trajectory collides with stable one and disappears.

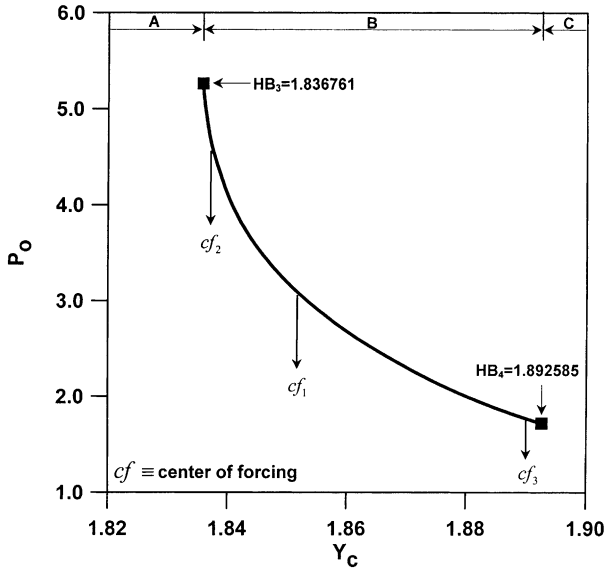

Fig. 7. Period of oscillation of the unforced reactor vs. dimensionless cooling coil temperature.

Fig. 8 also shows a period doubling region (PDR) is formed at the top of the resonance horn. The period doubling bifurcation occurs when a periodic trajectory becomes unstable by having one of its Floquet multipliers become more negative than -1, then the new trajectory remains periodic but has a period twice the period of the original trajectory. McKarnin et al. [30] have described in details the formation of such period doubling region. As the bottom of the period doubling region is crossed from below, the period $2P$ saddle which lie on the phased-locked torus collides with the unstable period $1P$ (this is the unstable limit cycle produced by forcing the unstable steady state), leaving only a period $1P$ saddle which separates the remaining period $2P$ nodes. As the forcing amplitude is increased further, the stable period

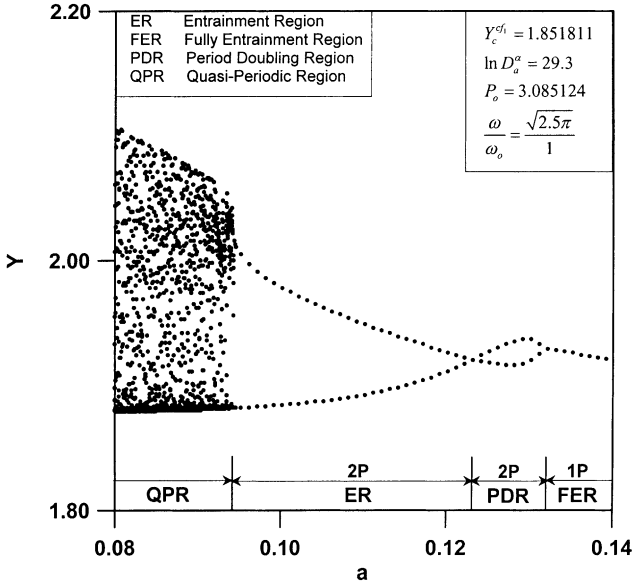

Fig. 9. One-parameter stroboscopic bifurcation diagram at $\omega/\omega_o = \sqrt{2.5\pi}/1$.

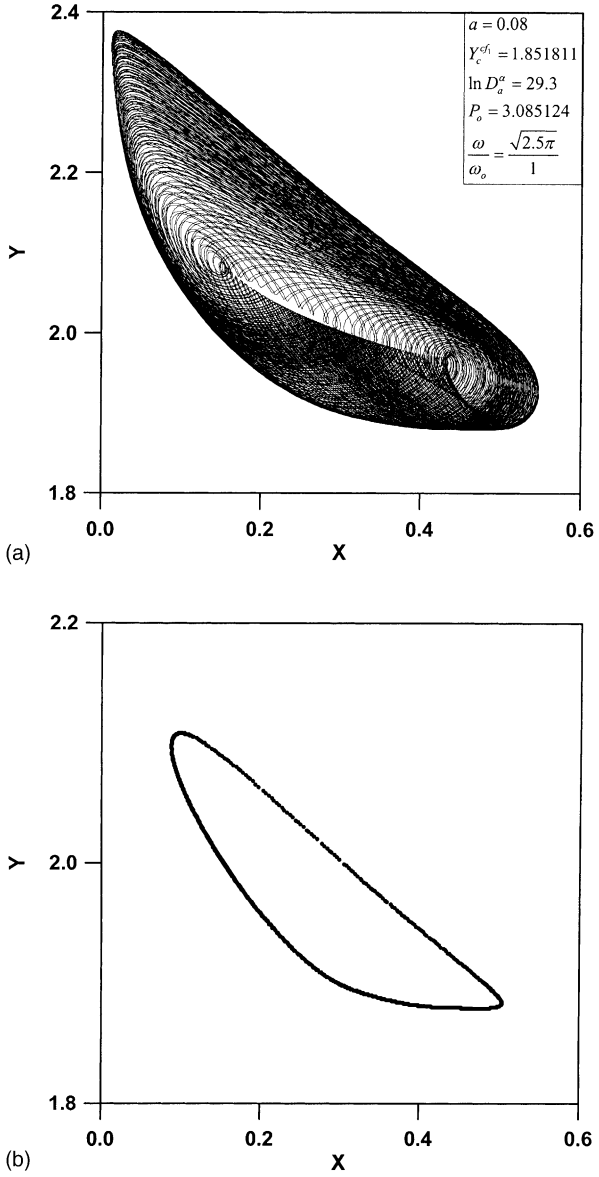

Fig. 10. Quasi-periodic phase plane of the forced reactor at $\omega/\omega_o = \sqrt{2.5\pi}/1$: (a) dynamic simulation phase plane; (b) stroboscopic phase plane.

2*P* node collides with the period 1*P* saddle as the top of the period doubling curve is crossed to leave only stable period 1*P* node i.e. the system overpowered by the external forcing. The region of the stable period 1*P* node is called fully entrainment region (FER) because the response of the forced reactor is periodic and its period equals to the forcing period (*P*). The crossing from period 2*P* to period 1*P* is period halving. Fig. 9 shows a one-parameter stroboscopic bifurcation diagram at $\omega/\omega_o = \sqrt{2.5\pi}/1 = 2.802495608/1$. It is clearly shown that as the forcing amplitude increases the system passes from a quasi-periodicity region (QPR) to a 2*P* (ER + PDR) regions and finally to a fully entrainment region (FER) of periodicity 1*P*.

The response of the forced reactor is called quasi-periodic when it has at least two incommensurate (their ratio is an irrational number) frequencies associated with it. The trajectories are constrained to the surface of a two-dimensional torus. In this case, the trajectory never repeats itself but is not chaotic i.e. the system does not exhibit sensitive dependence on initial conditions. Here, the Floquet multipliers form two complex conjugates cross the unit circle at an angle. Fig. 10(a) shows a quasi-periodic phase plane at $a = 0.08$ and $\omega/\omega_o = \sqrt{2.5\pi}/1 = 2.170803764/1$. The pattern of the stroboscopic phase plane of the quasi-periodic attractor looks like an invariant circle as shown in Fig. 10(b). The trajectory wanders complete over the surface of the torus. At large forcing amplitude the quasi-periodic trajectory bifurcates to fully entrainment region through a Hopf bifurcation point of the stroboscopic map as shown in Fig. 8. At the Hopf bifurcation point, the Floquet multipliers lie on the unit circle in the complex plane. The Hopf bifurcation curves originate from points in the period doubling curve at which the Floquet multipliers are double −1. This is implies that the tori outside the resonance horn are fully entrained to 1*P* through the Hopf bifurcation points. Fig. 11 shows a one-parameter stroboscopic bifurcation diagram at $\omega/\omega_o = \sqrt{1.5\pi}/1 = 2.170803764/1$. The sequence of bifurcation events as the forcing amplitude is increased is quasi-periodicity, frequency locking region of periodicity 2*P*, quasi-periodicity and finally bifurcation to a fully entrainment region of periodicity 1*P* through a Hopf bifurcation.

Fig. 12 shows the effect of the position of the center of forcing (cf_1, cf_2, cf_3) on the resonance horn. It is interesting to note that the resonance horn decreases in size and its tip becomes sharper as the center of forcing moves from HB_1 to HB_2 shown in Figs. 6 and 7. This effect may be due to

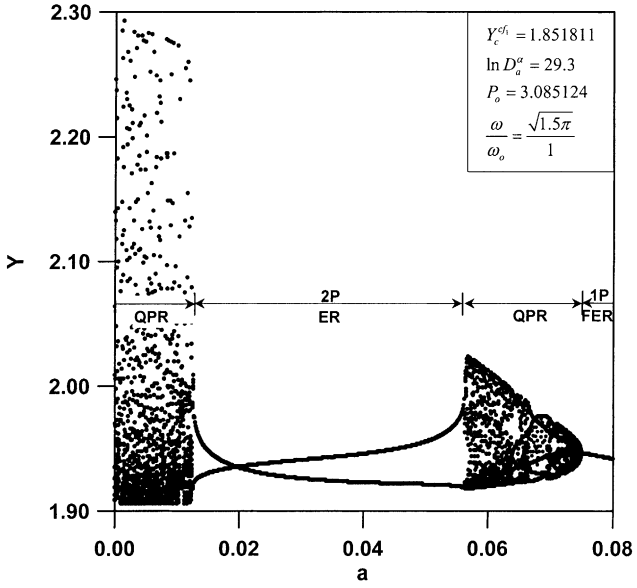

Fig. 11. One-parameter stroboscopic bifurcation diagram at $\omega/\omega_o = \sqrt{1.5\pi}/1$.

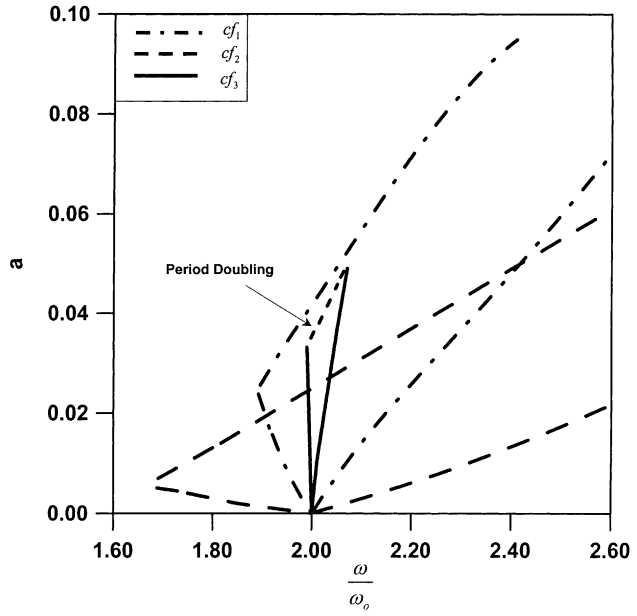

Fig. 12. Effect of the position of the center of forcing at $Y_c^{cf_1} = 1.851811$, $Y_c^{cf_2} = 1.837218$ and $Y_c^{cf_3} = 1.890070$ on the 2/1 resonance horn.

the decrease of the natural period of the autonomous system before forcing.

5. Conclusions

The steady state and dynamic behavior of two-phase systems in physical equilibrium in a continuous stirred tank reactor is investigated. In the range of parameters investigated, the two-parameters bifurcation analysis for the autonomous system shows that steady state multiplicity patterns not previously observed of isola and mushroom may develop in the neighborhood of a cusp (singular) point of codimension 2. It is also shown that the coincidence of two Hopf bifurcation points and Hopf and saddle-node points may occur forming degenerate singular points of codimension 2, which violate the non-singularity and transversality conditions of the hypotheses of classical Hopf theorem. It clear that, several important steady state features that are difficult to ascertain via numerical simulation are disclosed through the pseudo-arclength continuation technique.

The results of the non-autonomous system clearly show that the position of center of forcing relative to Hopf bifurcation points of the unforced reactor has a pronounced effect on the dynamic behavior of the forced reactor. Between the two extremes of the frequency locking region and fully entrainment region in the excitation diagram, complex dynamic behavior of the forced system may occur.

Despite the fact that the results reported in this paper for limited regions in the parameter space, it seems satisfactory to reflect the richness and complexity of the dynamic behavior of this system. It would be interested to confirm the results obtained here by well-designed experiments.

References

[1] L.K. Doraiswamy, M.M. Sharma, Heterogeneous reactions: analysis, examples, and reactor design, Fluid–Fluid–Solid Reactions, vol. 2, Wiley, USA, 1984.
[2] R.A. Schmitz, N.R. Amundson, An analysis of chemical reactor stability and control. Va. Two-phase systems in physical equilibrium. 1, Chem. Eng. Sci. 18 (1963) 265.
[3] M.E. Abashar, M.R. Judd, Synchronization of chaotic nonlinear oscillators: study of two coupled CSTRs, Chem. Eng. Sci. 53 (1998) 3741.
[4] A. Uppal, W.H. Ray, B.A. Poore, On the dynamic behavior of continuous stirred tank reactors, Chem. Eng. Sci. 29 (1974) 967.
[5] P. Gray, S.K. Scott, Autocatalytic reaction in the isothermal, continuous stirred tank reactor. Isola and other forms of multiplicity, Chem. Eng. Sci. 38 (1983) 29.
[6] P. Gray, S.K. Scott, Autocatalytic reactions in the isothermal, continuous stirred tank reactor, Chem. Eng. Sci. 39 (1984) 1087.
[7] V. Balakotaiah, D. Luss, Analysis of the multiplicity patterns of a CSTR, Chem. Eng. Commun. 13 (1981) 111.
[8] J.B. Planeaux, K.F. Jensen, Bifurcation phenomena in CSTR dynamics: a system with extraneous thermal capacitance, Chem. Eng. Sci. 41 (1986) 1497.
[9] F.I.C.C. Pais, A.A.T.G. Portugal, Steady state behaviour of isothermal two-phase continuous stirred tank reactors for extreme solids concentrations, Chem. Eng. Sci. 51 (1996) 321.
[10] S.S.E.H. Elnashaie, M.E. Abashar, Chaotic behavior of periodically forced fluidized bed catalytic reactors with consecutive exothermic chemical reactions, Chem. Eng. Sci. 49 (1994) 2483.
[11] M.E. Abashar, S.S.E.H. Elnashaie, Complex non-chaotic attractors in fluidized bed catalytic reactors, Trans. IChemE, Part A 75 (1997) 92.
[12] M.E. Abashar, S.S.E.H. Elnashaie, R. Hughes, Homoclinicity in the dynamics of forced fluidized bed catalytic reactors, Chaos Solitons Fract. 8 (1997) 1655.
[13] L.F. Galdden, M.D. Mantle, A.J. Sederman, E.H.L. Yuen, Magnetic resonance imaging of single-and two-phase flow in fixed bed reactors, Appl. Magnet. Reson. 22 (2002) 201.

[14] D. Luss, B. Marwaha, Hot-zone evolution and dynamics in heterogeneous catalytic systems, Chaos 12 (2002) 172.
[15] R.A. Schmitz, N.R. Amundson, An analysis of chemical reactor stability and control. Vb. Two-phase systems in physical equilibrium. 2, Chem. Eng. Sci. 18 (1963) 391.
[16] C. Van Heerden, Autothermic processes, Ind. Eng. Chem. 45 (1953) 1242.
[17] M. Kubicek, M. Marek, Computational Methods in Bifurcation Theory and Dissipative Structures, Springer, New York, 1983.
[18] M. Golubitsky, D. Schaeffer, A theory for imperfect bifurcation via singularity theory, Commun. Pure Appl. Math. 32 (1979) 1.
[19] M. Golubitsky, D.G. Schaeffer, Singularity and Groups in Bifurcation Theory, Springer, New York, 1985.
[20] M. Golubitsky, B.L. Keyfitz, A qualitative study of the steady state solutions for a continuos flow stirred tank chemical reactor, SIAM J. Math. Anal. 11 (1980) 316.
[21] V. Balakotaiah, D. Luss, Exact steady-state multiplicity criteria for two consecutive or parallel reactions in lumped-parameter systems, Chem. Eng. Sci. 37 (1982) 433.
[22] V. Balakotaiah, D. Luss, Structure of the steady-state solutions of lumped-parameter chemically reacting systems, Chem. Eng. Sci. 37 (1982) 1611.
[23] V. Balakotaiah, D. Luss, Multiplicity features of reacting systems. Dependence of the steady-states of a CSTR on the residence time, Chem. Eng. Sci. 38 (1983) 1709.
[24] R. Gilmore, Catastrophe Theory for Scientists and Engineers, Wiley, New York, 1981.
[25] M.E.E. Abashar, Bifurcation, instability and chaos in fluidized bed catalytic reactors, Ph.D. Thesis, The University of Salford, UK, 1994.
[26] D. Sincic, J.E. Bailey, Pathological dynamic behavior of forced periodic chemical processes, Chem. Eng. Sci. 32 (1977) 281.
[27] I.G. Kevrekidis, R. Aris, L.D. Schmidt, The stirred tank forced, Chem. Eng. Sci. 41 (1986) 1549.
[28] I.G. Kevrekidis, R. Aris, L.D. Schmidt, Some common features of periodically forced reacting systems, Chem. Eng. Sci. 41 (1986) 1263.
[29] G.A. Cordonier, L.D. Schmidt, R. Aris, Forced oscillations of chemical reactors with multiple steady states, Chem. Eng. Sci. 45 (1990) 1659.
[30] M.A. McKarnin, L.D. Schmidt, R. Aris, Response of non-linear oscillations to forced oscillations, Chem. Eng. Sci. 43 (1988) 2833.
[31] E. Doedel, J.P. Kernévez, AUTO: Software for Continuation and Bifurcation Problems in Ordinary Differential Equations, California Institute of Technology, Pasadena, California, 1986.
[32] P. Trambouz, Reactor design relations for two-phase liquid–liquid processes, Chem. Eng. Sci. 14 (1961) 161.
[33] User's Manual, Fortran Subroutines for Mathematics and Statistics, vol. 1, Dgear 1-10. IMSL Inc., Houston, TX, 1985.